Giant Goos-Hänchen shift using $\mathcal{PT}$ symmetry

Ziauddin,[1,2,*] You-Lin Chuang,[1] and Ray-Kuang Lee[1,3,†]

[1]*Institute of Photonics and Technologies, National Tsing-Hua University, Hsinchu 300, Taiwan*

[2]*Department of Physics, COMSATS Institute of Information Technology, Islamabad, Pakistan*

[3]*Physics Division, National Centre of Theoretical Science, Hsinchu 300, Taiwan*

(Received 8 March 2015; published 8 July 2015)

Influence of $\mathcal{PT}$ symmetry on the Goos-Hänchen (GH) shift in the reflected light is presented for an ensemble of atomic medium in a cavity, in the configuration of four-level N-type (^{87}Rb atoms) systems driving by two copropagating strong laser fields and a weak probe field. The atom-field interaction follows the realization of $\mathcal{PT}$ symmetry by adjusting the coupling field detunings [J. Sheng*et al.*, Phys. Rev. A **88**, 041803(R) (2013)]. A giant enhancement for the GH shift in the reflected light is revealed when the $\mathcal{PT}$-symmetry condition is satisfied.

DOI: 10.1103/PhysRevA.92.013815 PACS number(s): 42.25.Bs, 42.50.Gy, 11.30.Er, 78.20.Ci

I. INTRODUCTION

The Goos-Hänchen (GH) shift is the lateral displacement of an optical beam from its expected geometrical optics path. The existence of this shift was first observed experimentally by Goos and Hänchen in 1947 [1] in total internal reflection from the interface of two different media. Since then, a lot of different schemes have been suggested by the researchers to study the GH shift [2–9]. Nowadays, the GH shift and its applications have attracted a lot of attentions in various fields of science, involving micro- and nanostructures [10], quantum and plasma physics [11], scientific research in graphene [12,13], sensors [14,15], and phase-conjugate mirrors [16]. The GH shift has also been applied in optical sensing, for example, measuring refractive index, beam angle, irregularities, and roughness on the surface of dispersive medium [7,17] using the tunable GH with a fix configuration. The tunable GH shift in the reflected light has been investigated for a fixed cavity using different atomic systems in recent years [18–24]. The notable point in all these investigations is that in the optical regime the measurement of the GH shift is a difficult task due to its small magnitude. Therefore, from an application point of view, it will be more valuable to enhance the magnitude of GH shift via some external parameters. Recently, the amplitude control of the GH shift has been studied via Kerr field in the optical regime [22]. In that work a four-level atomic system was considered and the effect of Kerr nonlinearity of the group index was investigated. They found that the group index was enhanced by increasing the strength of Kerr field. The enhancement of group index then led to a change in the amplitude of the GH shifts.

In addition, in recent years a lot of attention has been focused on a class of non-Hermitian Hamiltonians with $\mathcal{PT}$ symmetry. The concept of $\mathcal{PT}$ symmetry was first considered by Bender and Boettcher in 1998 [25]. They discovered the existence of complex potentials of the Schrödinger equation having real spectra and related this property to the parity and time symmetries of physical systems. When the potential satisfies the condition $V(x) = V^*(-x)$, the Hamiltonian becomes $\mathcal{PT}$ symmetric. Then the real and imaginary parts of the potential must be even and odd functions of position, respectively. Further, the $\mathcal{PT}$ symmetry was studied using the concept of gain and loss in the systems [26–29]. In optics, the $\mathcal{PT}$ symmetry demands that the refractive index of the system must have the condition, i.e., $n(r) = n^*(-r)$. This was first experimentally observed by Rüter and coworkers using four-wave mixing in a Fe-doped ($LiNbO_3$) substrate [30]. There are practical applications to the realization of optical $\mathcal{PT}$-symmetry potential; these include, for example, nonreciprocal propagation of wave [30–33], implementation of coherent perfect absorber [34,35], and giant wave amplification [36].

Recently, Hang and coworkers suggested a scheme [37] and studied the realization of $\mathcal{PT}$ symmetry by considering an atomic gas consisting of two species of Λ configuration. This investigation is relatively different from solid-state systems as stated above [30–36], and has many attractive characteristics over solid-state systems. For example, the optical structures can be controlled via different external parameters, i.e., Rabi frequencies, detunings, and pump fields. In this investigation [37], the $\mathcal{PT}$-symmetry refractive index is valid in the whole space and can be controlled by changing the external parameters of the proposed system. Since then, some other proposals have been investigated based on atomic systems [38,39]. In these investigations a single specie is considered and the realization of $\mathcal{PT}$ symmetry in each case is studied. In a $\mathcal{PT}$-symmetric medium the gain and loss balance each other and the light propagates farther in the medium as compared to non-$\mathcal{PT}$-symmetric medium. Now, it will be more valuable to proceed with the idea of $\mathcal{PT}$ symmetry and study its influence on the GH shift.

In the present article, we consider a $\mathcal{PT}$-symmetric medium and study its influence on the GH shift. The motivation comes from an earlier work, where a four-level N-type atomic configuration has been considered [39] and the realization of the $\mathcal{PT}$ symmetry in atomic medium under an electromagnetically induced transparency (EIT) was shown. We consider this atomic model and study the influence of $\mathcal{PT}$ symmetry on the GH shift. It is well known from the realization of $\mathcal{PT}$ symmetry that the gain and loss balance each other effect. The balance of gain and loss in a system then leads to provide a real wave propagation constant and the light penetrates more into the medium. Here, we study the effect of $\mathcal{PT}$ symmetry on the GH shift and expect a giant GH shift in the reflected light for $\mathcal{PT}$ symmetry.

II. MODEL

We consider a system consisting of three layers, labeled as 1, 2, and 3, as depicted in the figures. Layers 1 and 3 are walls

*ziauddin@comsats.edu.pk

†rklee@ee.nthu.edu.tw

of the system having thickness d_1, each with permittivity ϵ_1. Layer 2 is considered as the atomic medium of N-type atoms with thickness d_2 and permittivity ϵ_2. The permittivity of the medium 2 is directly related to the refractive index of the medium. A TE-polarized light with large width is incident on the system, making an angle θ with the z axis. Two strong coherent fields and one weak probe field are applied to drive the four-level atomic system in an EIT configuration. The incident probe light field is reflected or transmitted through the system with a lateral GH shift. The GH shift in the reflected and transmitted light can be calculated using the stationary phase theory [18,19] as

$$S_{r,t} = -\frac{\lambda_p}{2\pi}\frac{d\varphi_{r,t}}{d\theta}, \tag{1}$$

where $\varphi_{r,t}$ is the phase of the reflection and transmission coefficients. Explicitly, the corresponding GH shift in the reflected and transmitted probe light beam can be expressed in the forms as [18,19]

$$S_r = -\frac{\lambda_p}{2\pi\,|r(k_x,\omega_p)|^2}\left\{\mathrm{Re}[r(k_x,\omega_p)]\frac{d\mathrm{Im}[r(k_x,\omega_p)]}{d\theta} - \mathrm{Im}[r(k_x,\omega_p)]\frac{d\mathrm{Re}[r(k_x,\omega_p)]}{d\theta}\right\} \tag{2}$$

and

$$S_t = -\frac{\lambda}{2\pi\,|t(k_y,\omega_p)|^2}\left\{\mathrm{Re}[t(k_y,\omega_p)]\frac{d\mathrm{Im}[t(k_y,\omega_p)]}{d\theta} - \mathrm{Im}[t(k_y,\omega_p)]\frac{d\mathrm{Re}[t(k_y,\omega_p)]}{d\theta}\right\}. \tag{3}$$

where $r(k_x,\omega_p)$ and $t(k_y,\omega_p)$ are the reflection and transmission coefficients. In our configuration, the input and output of the electric fields associated with propagation of light through a multilayered structure can be related to each other using a transfer matrix approach [19]

$$m_j(k_y,\omega_p,d_j) = \begin{pmatrix} \cos(k_j^z d_j) & i\sin(k_j^z d_j)/q_j \\ iq_j\sin(k_j^z d_j) & \cos(k_j^z d_j) \end{pmatrix}, \tag{4}$$

where

$$k_j^z = k\sqrt{\epsilon_j - \sin^2\theta} \tag{5}$$

is the z component of wave number, $k = \omega/c$ in vacuum, c is the speed of light, $q_j = k_j^z/k$, d_j is the thickness, and j labels the jth layer of the medium. For the configuration illustrated in Fig. 1(a), our system consists of three layers: 1 and 3 are the cavity walls and 2 is the intracavity medium. The total transfer matrix can therefore be written as

$$Q(k_y,\omega_p) = m_1(k_y,\omega_p,d_1)m_2(k_y,\omega_p,d_2)m_1(k_y,\omega_p,d_1),$$

and the reflection and transmission coefficients are therefore calculated as

$$r(k_y) = \frac{q_0(Q_{22}-Q_{11}) - \left(q_0^2Q_{12}-Q_{21}\right)}{q_0(Q_{22}+Q_{11}) - \left(q_0^2Q_{12}+Q_{21}\right)},$$

$$t(k_y) = \frac{2q_0}{q_0(Q_{22}+Q_{11}) - \left(q_0^2Q_{12}+Q_{21}\right)},$$

where Q_{ij} are the elements of the total transfer matrix $Q(k_y,\omega_p)$ and $q_0 = \sqrt{\epsilon_0 - \sin^2\theta}$. Here, the permitivity (ε_1) of the layers 1 and 3 is assumed to be constant, while the permitivity (ε_2) and susceptibility (χ) of the intracavity medium are defined via the relation [18,19]

$$\varepsilon_2 = 1 + \chi. \tag{6}$$

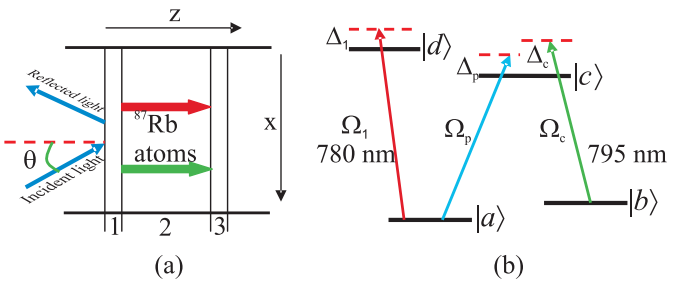

FIG. 1. (Color online) (a) The schematics of the light incident on a cavity and (b) the energy-level configuration of an N-type system.

A. Atom field interaction

To take possible experimental realization into consideration, here we consider an atomic ensemble of ^{87}Rb atoms in the four-level N-type configuration. The corresponding energy levels are denoted as $|a\rangle$, $|b\rangle$, $|c\rangle$, and $|d\rangle$; see Fig. 1(b). The energy levels are considered from the D_1 line of ^{87}Rb atoms, with $|a\rangle = |5S_{1/2}, F = 1\rangle$, $|b\rangle = |5S_{1/2}, F = 2\rangle$, $|c\rangle = |5P_{1/2}, F' = 1\rangle$, and $|d\rangle = |5P_{3/2}, F' = 2\rangle$. The probe, coupling, and pumping fields couple with the transitions $|a\rangle \leftrightarrow |c\rangle$, $|b\rangle \leftrightarrow |c\rangle$, and $|a\rangle \leftrightarrow |d\rangle$, respectively. The two pump and coupling fields are propagating in the z direction, which make two coupled waveguide structures. The waveguide structure of two fields provide gain and loss in a system simultaneously. The probe field propagates through the medium, which makes an angle θ with the z axis.

The density matrix equations for the N-type atomic configuration under the rotating wave approximation can therefore be written [39] as

$$\begin{aligned}
\dot\rho_{bb} &= \Gamma_{db}\rho_{dd} + \Gamma_{cb}\rho_{cc} - \Gamma_{ba}\rho_{bb} + \frac{i}{2}(\Omega_c^*\rho_{cb} - \Omega_c\rho_{bc}),\\
\dot\rho_{cc} &= \Gamma_{dc}\rho_{dd} - \Gamma_{cb}\rho_{cc} - \Gamma_{ca}\rho_{cc}\\
&\quad + \frac{i}{2}(\Omega_c\rho_{bc} - \Omega_c^*\rho_{cb} + \Omega_p\rho_{ac} - \Omega_p^*\rho_{ca}),\\
\dot\rho_{dd} &= -(\Gamma_{dc} + \Gamma_{db} + \Gamma_{da})\rho_{dd} + \frac{i}{2}(\Omega_1\rho_{ad} - \Omega_1^*\rho_{da}),\\
\dot\rho_{ba} &= -\tilde\gamma_{ba}\rho_{ba} + \frac{i}{2}\Omega_c^*\rho_{ca} - \frac{i}{2}\Omega_1\rho_{bd} - \frac{i}{2}\Omega_p\rho_{bc},\\
\dot\rho_{ca} &= -\tilde\gamma_{ca}\rho_{ca} + \frac{i}{2}\Omega_c\rho_{ba} - \frac{i}{2}\Omega_1\rho_{cd} + \frac{i}{2}(\rho_{aa} - \rho_{cc})\Omega_p,\\
\dot\rho_{da} &= -\tilde\gamma_{da}\rho_{da} - \frac{i}{2}\Omega_p\rho_{dc} + \frac{i}{2}(\rho_{aa} - \rho_{dd})\Omega_1,\\
\dot\rho_{cb} &= -\tilde\gamma_{cb}\rho_{cb} + \frac{i}{2}\Omega_p\rho_{ab} + \frac{i}{2}(\rho_{bb} - \rho_{cc})\Omega_c,\\
\dot\rho_{db} &= -\tilde\gamma_{db}\rho_{db} - \frac{i}{2}\Omega_c\rho_{dc} + \frac{i}{2}\Omega_1\rho_{ab},\\
\dot\rho_{dc} &= -\tilde\gamma_{dc}\rho_{dc} + \frac{i}{2}\Omega_1\rho_{ac} - \frac{i}{2}\Omega_c^*\rho_{db} - \frac{i}{2}\Omega_p^*\rho_{da},
\end{aligned} \tag{7}$$

where Ω_p, Ω_1, and Ω_c are the Rabi frequencies of probe, pump, and coupling fields, respectively, whereas $\tilde{\gamma}_{ba} = \gamma_{ba} - i(\Delta_p - \Delta_c)$, $\tilde{\gamma}_{ca} = \gamma_{ca} - i\Delta_p$, $\tilde{\gamma}_{da} = \gamma_{da} - i\Delta_1$, $\tilde{\gamma}_{cb} = \gamma_{cb} - i\Delta_c$, $\tilde{\gamma}_{db} = \gamma_{db} - i(\Delta_c + \Delta_1 - \Delta_p)$, and $\tilde{\gamma}_{dc} = \gamma_{dc} - i(\Delta_1 - \Delta_p)$. Here, Γ_{nm} is the decay between level $|n\rangle$ and $|m\rangle$; and $\gamma_{nm} = (\Gamma_m + \Gamma_n)/2$.

Using the density matrix equations (7) one can find the optical susceptibility of the proposed atomic configuration numerically. The optical susceptibility can be calculated using the expression $\chi = \frac{2N\mu_{ac}}{\epsilon_0 E_p}\rho_{ca}$. The refractive index of the medium can therefore be written as

$$n = \sqrt{1+\chi} \cong 1 + \frac{\chi}{2}. \tag{8}$$

The refractive index of the medium can also be expressed as $n = n_0 + n_r + in_i$, where n_r and n_i are the real and imaginary parts of the refractive index, respectively, whereas $n_0 = 1$ is the background refractive index of the medium. From Eqs. (5)–(8), one can find that the reflection and transmission coefficients depend on the permittivities of the cavity walls and intracavity medium, i.e., ϵ_1 and ϵ_2, respectively. As a result, the GH shifts in the reflected and transmitted probe light beams also depend on the permittivities of the cavity wall and the intracavity medium.

The realization of $\mathcal{PT}$ symmetry was studied in N-type atomic configuration [39] by employing two different laser fields side by side. Each laser field has a Gaussian intensity while the probe field varies in the transverse direction. Now the total intensity distribution of the coupling beams can be represented as

$$I_c(x) = A(e^{\frac{-(x-a)^2}{2\sigma^2}} + e^{\frac{-(x+a)^2}{2\sigma^2}}), \tag{9}$$

where A and $2a$ are constant and separation between the two laser fields, respectively.

III. RESULTS AND DISCUSSION

A. Manipulation of the refractive index using $\mathcal{PT}$ symmetry

The realization of $\mathcal{PT}$ symmetry was established cleverly by adjusting the coupling detunings. In optics, $\mathcal{PT}$ symmetry requires that there will be gain and loss simultaneously in a system, and also the real and imaginary parts of the refractive index of the medium must be even and odd, respectively. In the present scheme, two different detunings are considered and simultaneously introduced gain and loss in two wave guides. By adjusting the detunings of the two wave guides carefully, one can investigate the $\mathcal{PT}$ symmetry and non-$\mathcal{PT}$-symmetry in the system. The parameters $\Gamma_{db} = \Gamma_{cb} = \Gamma_{ca} = 6\pi, \Gamma_{ba} = \Gamma_{dc} = \Gamma_{da} = 0, \Omega_1 = 6\pi, \Omega_p = 0.2\pi, a = 10, \sigma = 3$ are considered and remained fixed, while the detunings of the coupling fields are adjusted carefully for the realization of $\mathcal{PT}$ symmetry. Here, we consider two detunings, i.e., $\Delta_c/2\pi = -1.7000$ MHz and -1.7155 MHz and plot the real and imaginary parts of the refractive index versus x; see Fig. 2. We know from the requirement of $\mathcal{PT}$ symmetry that the real and imaginary parts of the refractive index must be even and odd, respectively, and the gain and loss must balance each other. The imaginary part in Fig. 2(b) does not fulfill the condition of $\mathcal{PT}$ symmetry due to the fact that the gain and loss do not balance each other. By adjusting the coupling field detunings as described in Ref. [39], one can achieve the $\mathcal{PT}$-symmetric refractive index, i.e., $n(x) = n^*(-x)$. To achieve the realization of $\mathcal{PT}$ symmetry, we adjust the two detunings as $\Delta_c/2\pi = -1.7137$ MHz and -1.7155 MHz and plot the real and imaginary parts versus x again; see Fig. 3. In the plot the real and imaginary parts of the refractive index are even and odd, respectively. It is also obvious from the imaginary part of the refractive index that the gain and loss balance each other. From this one can conclude that at this condition the medium behaves as a $\mathcal{PT}$-symmetric medium.

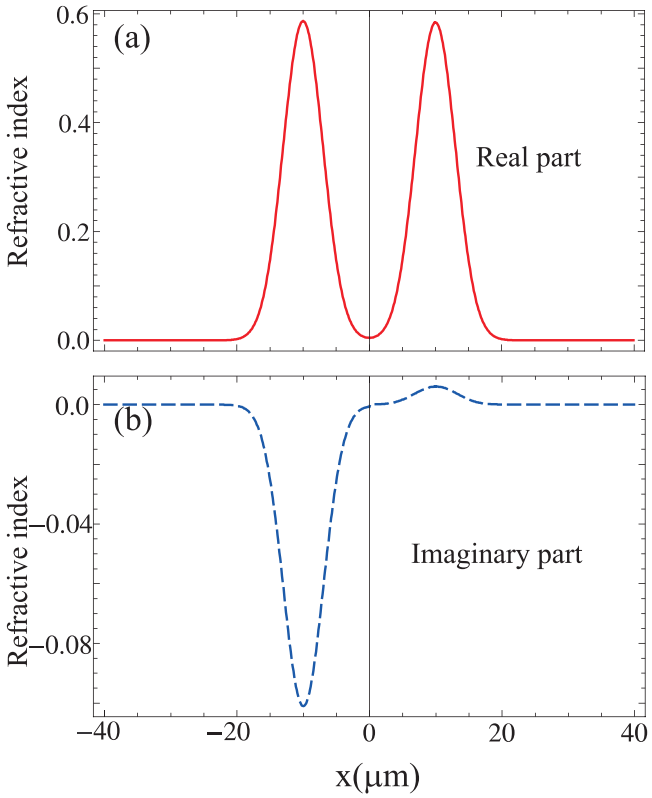

FIG. 2. (Color online) (a) The real and (b) imaginary parts of the refractive index vs position x. The parameters used are $\Gamma_{db} = \Gamma_{cb} = \Gamma_{ca} = 6\pi, \Gamma_{ba} = \Gamma_{dc} = \Gamma_{da} = 0, \Omega_1/\pi = 6$ MHz, $\Omega_p/\pi = 0.2$ MHz, $a = 10, \sigma = 3$, $\Delta_c/2\pi = -1.7000$ MHz, and -1.7155 MHz.

Now, to see a more clear picture of non-$\mathcal{PT}$ and $\mathcal{PT}$ symmetry, we consider the probe field propagation in the z direction and we show that the propagation constant is almost real value under $\mathcal{PT}$-symmetry condition. Using the paraxial approximation we can write down the field equation [37] as

$$i\frac{\partial \mathcal{E}_p}{\partial z} + \frac{1}{2k_p}\frac{\partial^2 \mathcal{E}_p}{\partial x^2} + \frac{1}{2}k_p\chi_p(x)\mathcal{E}_p = 0, \tag{10}$$

where k_p is the wave vector of probe field and

$$\mathcal{E}_p(z,x) = E(x)e^{ibz}, \tag{11}$$

with b being the propagation constant. The propagation constant in Eq. (11) clearly shows that the field would be attenuated quickly during propagation in the medium when b has a large imaginary part. In contrast, the field can propagate

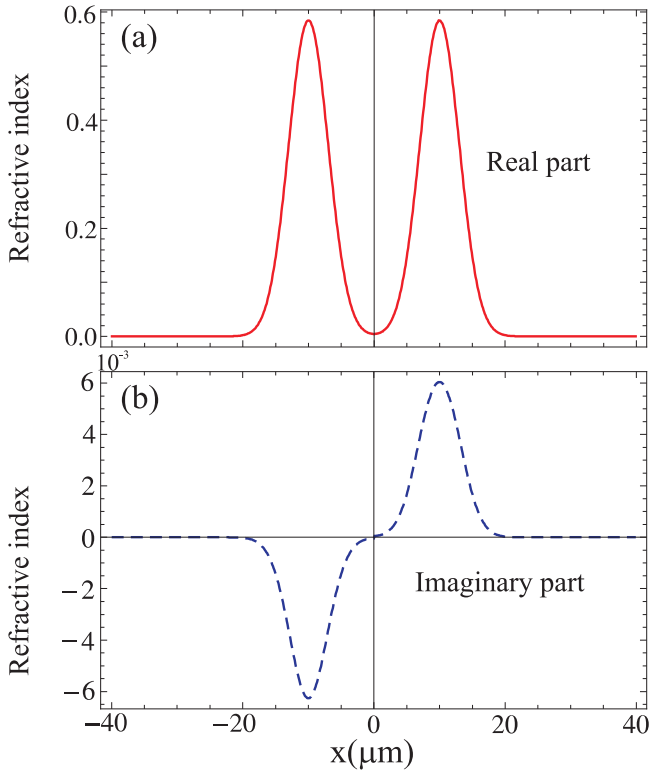

FIG. 3. (Color online) (a) The real and (b) imaginary parts of the refractive index vs position x for $\Delta_c/2\pi = -1.7137$ MHz and -1.7155 MHz. The other parameters are the same as in Fig. 2.

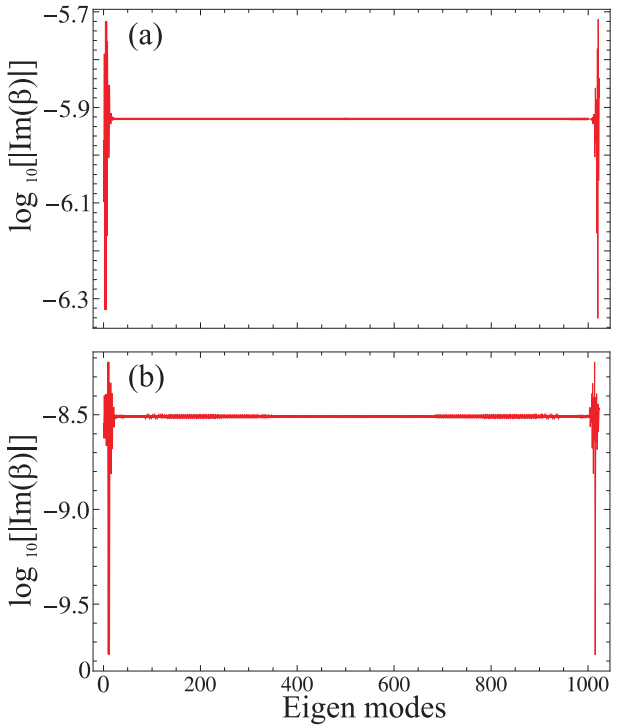

FIG. 4. (Color online) The spectrum of eigenvalue of $\log_{10}[\mathrm{Im}(\beta)]$ vs different eigenmodes for (a) non-$\mathcal{PT}$ and (b) $\mathcal{PT}$ symmetry.

for longer distances if the imaginary part of b is small. To study the field attenuation behavior in the medium, we can solve the eigenvalue problem instead of solving the field equation. Thus we substitute Eq. (11) into Eq. (10) and after simplification we get the eigenvalue equation as

$$\frac{dE}{d\xi^2} + \frac{k_p}{k_s^2}\chi(\xi) = \beta E, \tag{12}$$

where $\beta = \frac{2k_p}{k_s^2}b$. To show the spectrum of β, we plot the $\mathrm{Im}(\beta)$ in $\log_{10}$ scale versus different numbers of eigenmodes for two different conditions, i.e., for non-$\mathcal{PT}$ and $\mathcal{PT}$ symmetric; see Fig. 4. In Fig. 4(a), we plot the $\mathrm{Im}(\beta)$ by considering the non-$\mathcal{PT}$-symmetric case and keep all the parameters as the same as considered in Fig. 2. Next, we choose all the parameters as considered in Fig. 3 for $\mathcal{PT}$-symmetric case and plot again the $\mathrm{Im}(\beta)$ versus eigenmodes. The plot shows that the $\mathrm{Im}(\beta)$ decreases. Comparing the two situations above, we can clearly find out that there is almost 1000 times difference between non-$\mathcal{PT}$ and $\mathcal{PT}$-symmetric cases.

B. Influence of $\mathcal{PT}$ symmetry on the GH shift in the reflected light

In this section, we study the influence of $\mathcal{PT}$ symmetry on the GH shift in the reflected and transmitted lights. We expect that the amplitude of the GH shift in the reflected light increases when the $\mathcal{PT}$-symmetry condition is satisfied in a system. To best of our knowledge, no one can address the influence of $\mathcal{PT}$ symmetry on the GH shift. Using Eqs. (2) and (3), we study the GH shift for two different conditions, i.e., non-$\mathcal{PT}$ and $\mathcal{PT}$ symmetry. Initially, we consider a non-$\mathcal{PT}$-symmetric case as described in Fig. 2 and study the GH shift. We plot the GH shift in the reflected and transmitted light versus incident angle θ ranging from 0.1 to 0.3 rad for simplicity; see Fig. 5(a). At incident angle $\theta = 0.21$ rad positive shifts in the reflected and transmitted light are observed. To study more about the GH shift, we plot the absolute of reflection coefficient and phase shift versus incident angle θ; see Fig. 5(b). The dip in the reflection curve at incident angle $\theta = 0.21$ rad corresponds to the resonance condition. The inset in Fig. 5(b) show the phase shift in the reflected light, which shows a phase change at and around incident angle $\theta = 0.21$ rad. Next, we consider a $\mathcal{PT}$-symmetric case as described in Fig. 3 and study its influence on the GH shift in the reflected and transmitted light. We again plot the GH shift versus incident angle θ ranging from 0.1 to 0.3 rad; see Fig. 6(a). A giant GH shift in the reflected light appears at incident angle $\theta = 0.21$ rad due to $\mathcal{PT}$ symmetry in a medium. The GH shift in the transmitted light is very small as compared to the GH shift in the reflected light; see the inset in Fig. 6(a). We also calculate the group index of the total cavity using the relation $N_g \approx (1/L)d\varphi_{r,t}/d\omega_p$ [19]. The group indexes for the GH shifts in the reflected and transmitted beams are $N_g^r = 91.6$ and $N_g^t = 8.7$ for the non-$\mathcal{PT}$-symmetric case, respectively. In contrast, the group indexes for the GH shift in the reflected and transmitted lights are $N_g^r = 251.6$ and $N_g^t = 8.7$ for the $\mathcal{PT}$-symmetric case. It is obvious that the group index for the GH shift in the reflected light increases for the $\mathcal{PT}$-symmetric medium, while there is almost no change for the GH shift in the transmitted light. This is due to the fact that the GH

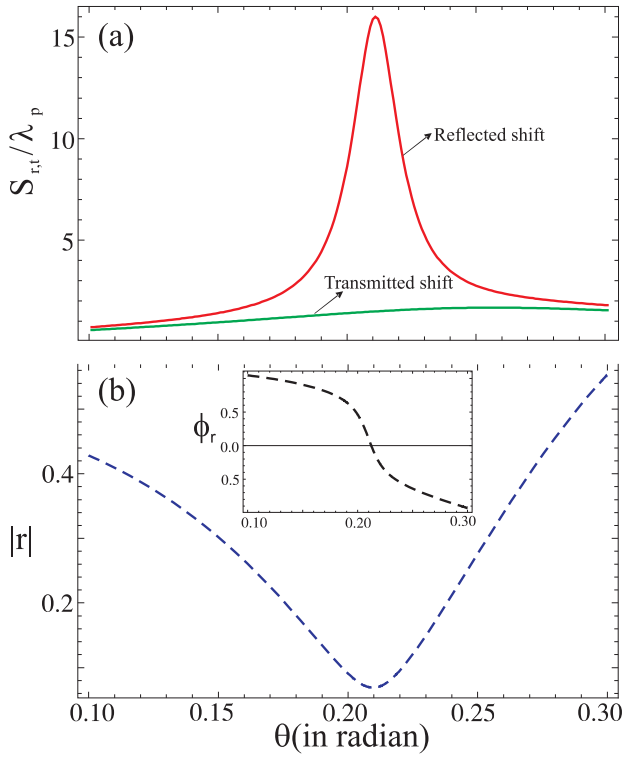

FIG. 5. (Color online) (a) The plot of GH shift in the reflected and transmitted light, and (b) the absolute reflection coefficient vs incident angle θ for $x = 0$, $d_1 = 0.2$ μm, $d_2 = 5$ μm, and $\epsilon_1 = 2.22$; all the other parameters are the same as in Fig. 2

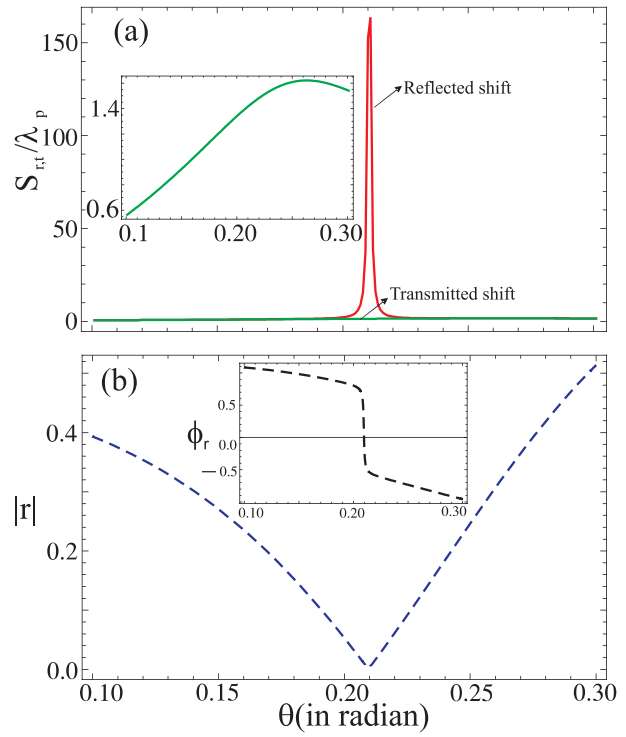

FIG. 6. (Color online) (a) The plot of GH shift in the reflected and transmitted light, and (b) the absolute reflection coefficient vs incident angle θ for $x = 0$, $d_1 = 0.2$ μm, $d_2 = 5$ μm, and $\epsilon_1 = 2.22$; all the other parameters are the same as in Fig. 3.

shift depends on the group index of the total cavity, which has been noticed earlier [19]. In comparison, the GH shift in the reflected light for $\mathcal{PT}$-symmetric case is enhanced 10 times as compared to the non-$\mathcal{PT}$-symmetric case. As described earlier, for $\mathcal{PT}$ symmetry the propagation constant is real, and the light propagates more into the medium. It is also well known from the literature that the GH shift is proportional to the penetration depth. This leads to a giant GH shift in the reflected light for $\mathcal{PT}$ symmetry. The absolute value for the reflection coefficient is also shown in Fig. 6(b). In the inset in Fig. 6(b) the phase shift of the reflected light is plotted versus incident angle θ. For the $\mathcal{PT}$-symmetric case the phase shift becomes very steep.

In the above discussion, we studied the GH shift in the reflected and transmitted lights for non-$\mathcal{PT}$ and $\mathcal{PT}$ symmetry based on the stationary phase theory [40] as mentioned earlier, so that the results and analysis are based on the fact that the incident light is considered is a plane wave. As discussed above, the $\mathcal{PT}$-symmetry realization in our system only affects the GH shift in the reflected light, and then it will be more valuable to show the above results of the GH shifts in the reflected light for a real system, when the incident light is a Gaussian profile with finite width. We show that our previous analysis and results of the GH shift in the reflected light are still valid when the incident light considered is a Gaussian beam. We follow the same approach as has been studied earlier in detail [18,20]. We can write the electric field for incident Gaussian light beam as

$$E_y^i(z,x) = \frac{1}{\sqrt{2\pi}} \int S(k_x) e^{i(k_z z + k_x x)} dk_x, \qquad (13)$$

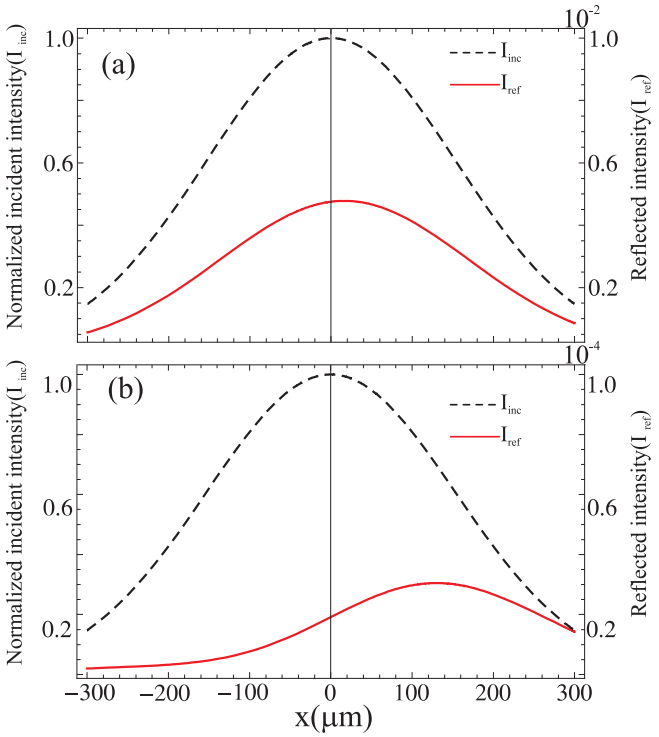

FIG. 7. (Color online) Intensity profiles for incident (I_{inc}) and reflected (I_{ref}) (a) non-$\mathcal{PT}$ and (b) $\mathcal{PT}$ symmetry.

where

$$S(k_x) = \frac{w_x}{\sqrt{2}} e^{-w_x^2(k_x - k_{x_0})^2/4} \tag{14}$$

is the angular spectrum of the Gaussian beam centered at $x = 0$ on the plane of $z = 0, k_{x_0} = k\sin(\theta)$, and $w_x = w\sec(\theta)$, where θ is the incident angle of the light beam. Then the reflected probe beams can therefore be written as

$$E_y^r(z,x)|_{z<0} = \frac{1}{\sqrt{2\pi}} \int r(k_x) S(k_x) e^{i(-k_z z + k_x x)} dk_x. \tag{15}$$

Using Eqs. (13) and (15) for the Gaussian incident light, we plot the intensity profiles of the incident (dashed curve) and reflected (solid curve) light beams. We consider a much longer half-width $w = 300\lambda_p$ as compared to its wavelength λ_p. We plot the intensity profiles for (i) non-$\mathcal{PT}$ and (ii) $\mathcal{PT}$ symmetry by considering an incident angle $\theta = 0.21$ rad in both cases. In earlier analysis of the GH shift in the reflected light, we investigated a positive GH shift in the reflected light at this incident angle in both cases; see Figs. 5(a) and 6(a). For the non-$\mathcal{PT}$-symmetry case, we plot the intensity profiles of the incident and reflected light beams; see Fig. 7(a). We investigate a similar behavior of the GH shift in the reflected light, as was observed previously in Fig. 5(a). Further, we consider the $\mathcal{PT}$-symmetry case and plot the intensity profiles of the incident and reflected light beams; see Fig. 7(b). The plot shows a similar control of the GH shift via $\mathcal{PT}$ symmetry as was investigated previously for a plane wave; compare Figs. 6(a) and 7(b). It is also investigated that the shapes of the reflected light are the same as those of the incident light beam when a relatively large width of the incident light is considered. From Fig. 7, we can conclude that our results are valid for a real system as well.

IV. CONCLUSION

In summary, by considering an ensemble of realistic cold atoms (D_1 line of ^{87}Rb N type) in a cavity we investigated the GH shift in the reflected and transmitted light for non-$\mathcal{PT}$- and $\mathcal{PT}$-symmetry cases, respectively. Using a stationary phase theory, the GH shift in the reflected light is revealed to be enhanced via $\mathcal{PT}$ symmetry whereas it remains unchanged in the transmitted light. It is due to the fact that in $\mathcal{PT}$ symmetry, the balance between gain and loss results in a giant change for the group index in the reflected light. Furthermore, a Gaussian light beam is also applied to confirm our results on the GH shift in the reflected light.

ACKNOWLEDGMENT

This work was supported by the Ministry of Science and Technology, Taiwan.

[1] F. Goos and H. Häncehn, Ann. Phys. (Leipzig) **1**, 333 (1947); **440**, 251 (1949).
[2] R. H. Renard, J. Opt. Soc. Am. **54**, 1190 (1964).
[3] D. K. Qing and G. Chen, Opt. Lett. **29**, 872 (2004).
[4] H. K. V. Lotsch, J. Opt. Soc. Am. **58**, 551 (1968).
[5] T. Tamir and H. L. Bertoni, J. Opt. Soc. Am. **61**, 1397 (1971).
[6] S. Chu and S. Wong, Phys. Rev. Lett. **48**, 738 (1982).
[7] J. L. Birman, D. N. Pattanayak, and A. Puri, Phys. Rev. Lett. **50**, 1664 (1983).
[8] A. Lakhtakia, Electromagnetics **23**, 71 (2003).
[9] P. R. Berman, Phys. Rev. E **66**, 067603 (2002).
[10] J. Soni, S. Mansha, S. D. Gupta, A. Banerjee, and N. Ghosh, Opt. Lett. **39**, 4100 (2014).
[11] S.-Y. Lee, J. Le Deunff, M. Choi, and R. Ketzmerick, Phys. Rev. A **89**, 022120 (2014).
[12] Q. Zhang and K. S. Chan, Appl. Phys. Lett. **105**, 212408 (2014).
[13] Z. H. Wu, F. Zhai, F. M. Peeters, H. Q. Xu, and K. Chang, Phys. Rev. Lett. **106**, 176802 (2011).
[14] Y.-Y. Nie, Y.-H. Li, Z.-J. Wu, X.-P. Wang, W. Yuan, and M.-H. Sang, Opt. Express **22**, 8943 (2014).
[15] X. Wang, C. Yin, J. Sun, H. Li, Y. Wang, M. Ran, and Z. Cao, Opt. Express **21**, 13380 (2013).
[16] B. M. Jost, A.-A. R. Al-Rashed, and B. E. A. Saleh, Phys. Rev. Lett. **81**, 2233 (1998).
[17] N. J. Harrick, Phys. Rev. Lett. **4**, 224 (1960).
[18] L. G. Wang, M. Ikram, and M. S. Zubairy, Phys. Rev. A **77**, 023811 (2008).
[19] Ziauddin, S. Qamar, and M. S. Zubairy, Phys. Rev. A **81**, 023821 (2010).
[20] Ziauddin and S. Qamar, Phys. Rev. A **84**, 053844 (2011).
[21] Ziauddin and S. Qamar, Phys. Rev. A **85**, 055804 (2012).
[22] M. Abbas, Ziauddin, and S. Qamar, Laser Phys. Lett. **11**, 015201 (2014).
[23] Ziauddin and S. Qamar, Opt. Commun. **319**, 1 (2014).
[24] Ziauddin, Y.-L. Chuang, and R.-K. Lee, Phys. Rev. A **91**, 013803 (2015).
[25] C. M. Bender and S. Boettcher, Phys. Rev. Lett. **80**, 5243 (1998).
[26] A. Ruschhaupt, F. Delgado, and J. D. Muga, J. Phys. A **38**, L171 (2005).
[27] C. M. Bender, D. C. Brody, and H. F. Jones, Phys. Rev. D **70**, 025001 (2004).
[28] I. Y. Goldsheid and B. A. Khoruzhenko, Phys. Rev. Lett. **80**, 2897 (1998).
[29] I. Rotter, J. Phys. A: Math. Theor. **42**, 153001 (2009).
[30] C. E. Rüter, K. R. Makris, R. El-Ganainy, D. N. Christodoulides, M. Segev, and D. Kip, Nat. Phys. **6**, 192 (2010).
[31] M. Kulishov, J. M. Laniel, N. Belanger, J. Azana, and D. V. Plant, Opt. Express **13**, 3068 (2005).
[32] Z. Lin, H. Ramezani, T. Eichelkraut, T. Kottos, H. Cao, and D. N. Christodoulides, Phys. Rev. Lett. **106**, 213901 (2011).
[33] L. Feng, Y.-L. Xu, W. S. Fegadolli, M.-H. Lu, J. E. B. Oliveira, V. R. Almeida, Y.-F. Chen, and A. Scherer, Nat. Mat. **12**, 108 (2013).
[34] S. Longhi, Phys. Rev. A **82**, 031801 (2010).

[35] Y. D. Chong, L. Ge, H. Cao, and A. D. Stone, Phys. Rev. Lett. **105**, 053901 (2010).
[36] V. V. Konotop, V. S. Shchesnovich, and D. A. Zezyulin, Phys. Lett. A **376**, 2750 (2012).
[37] C. Hang, G. Huang, and V. V. Konotop, Phys. Rev. Lett. **110**, 083604 (2013).
[38] H.-J. Li, J.-P. Dou, and G. Huang, Opt. Express **21**, 32053 (2013).
[39] J. Sheng, M. A. Miri, D. N. Christodoulides, and M. Xiao, Phys. Rev. A **88**, 041803(R) (2013).
[40] K. Artmann, Ann. Phys. **437**, 87 (1948); A. M. Steinberg and R. Y. Chiao, Phys. Rev. A **49**, 3283 (1994).